BEAMLINE DESIGN AND OPTIMISATION FOR HIGH INTENSITY MUON BEAMS AT PSI

Eremey Valetov*, Paul Scherrer Institut, CH-5232 Villigen PSI, Switzerland
(for the HIMB project)

Abstract

The High Intensity Muon Beams (HIMB) project at the Paul Scherrer Institute (PSI) will provide muon intensities of the order of 10^{10} muons/s for particle physics and material science experiments, two orders of magnitude higher than the state of the art, which is currently available also at PSI. In particle transport simulations for the HIMB, we use *G4beamline* with measured π^+ cross-sections and with variance reduction. We also use the codes *COSY INFINITY*, *TRANSPORT*, and *TURTLE* for some studies. We perform asynchronous Bayesian optimisation of the beamlines on a computing cluster using *G4beamline* and the optimisation package *DeepHyper*. We performed numerous studies for the design of the HIMB, and we produced various results, including the muon transmission, beam phase space, polarisation, and momentum spectrum.

INTRODUCTION

Next-generation muon experiments at the Paul Scherrer Institute (PSI), such as Mu3e phase II, require muons to be delivered at unprecedented rates. The Mu3e experiment [1] searches for indications of Beyond-Standard-Model physics by attempting to detect the neutrinoless decay of a muon into three electrons, which would be practically unobservable (at the 10^{-55} level) in the Standard Model of particle physics as a charged lepton flavour violation (cLFV) [2].

A next-generation $\mu \to e\gamma$ (MEG) experiment [3], searching for the highly suppressed cLFV decay of a muon into an electron and a photon, would also benefit from the substantially higher muon rates. Other intensity frontier particle physics experiments that would rely on an increase in the available muon rates are envisaged [3].

In addition to particle physics, novel concepts for performing characterisations of samples using the muon spin rotation method (μSR) such as pixel-based detectors or microbeams also require an increase in available muon rate [3].

With the presently available rate of $\sim 10^8$ muons/s, to achieve the sensitivity of 10^{-16}, phase II of the Mu3e experiment would have to run for more than 13 years. The High Intensity Muon Beams (HIMB) project [4] seeks to deliver muons at $\sim 10^{10}$ muons/s at a proton current of 2.4 mA, making such sensitivities feasible [3].

To provide a high-intensity muon beam at 10^{10} muons/s into the experimental areas, the HIMB project will use a new graphite target "TgH" with a slanted target design, which increases the surface muon rate; high-acceptance capture solenoids close to the target; and solenoid focusing instead of quadrupole focusing in the beamlines MUH2 and MUH3

---

* eremey.valetov@psi.ch

for a higher transmission rate. A partial layout of the HIMB is shown in Fig. 1. The MUH2 beamline has only solenoid focusing, while the MUH3 beamline has solenoid focusing in the first two straight sections and conventional quadrupole focusing further downstream. The HIMB will also benefit from a newly designed layout that uses lower bending angles and large-aperture dipoles.
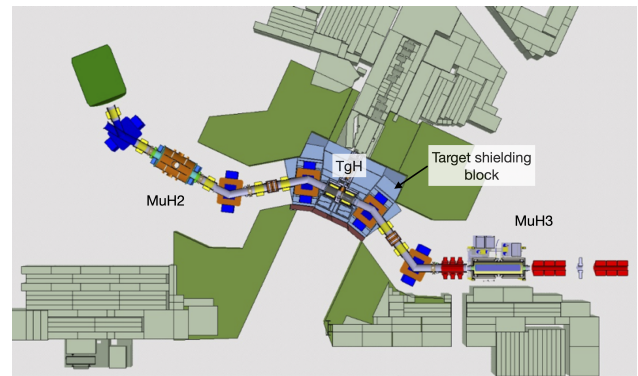

Figure 1: Layout of the HIMB target station and beamlines. The MUH3 beamline is not fully shown; it extends about 38 m from target TgH to the final focus of its branch MUH3.3 and also has a branch MUH3.2.

We performed optimisations, studies, modelling, and simulations for the target station and the muon beamlines of the HIMB project.

The scope of this paper is the author's collaborative contributions to the HIMB project. For further information about the project, please see the IMPACT conceptual design report [4]. The IMPACT project comprises the HIMB and the TATTOOS projects.

PARTICLE TRANSPORT

For simulations of particle transport and the production of surface muons at the target station, we mainly use *G4beamline* [5], based on a custom build of *Geant4* [6] with PSI's own measured π^+ cross-sections [7] and a splitting factor for π^+ production and decay for variance reduction. The measured cross-sections were found to be more precise than the default *Geant4* cross-sections, which deviated from the experimental data by a factor of up to ten (see Ref. [7]). The new target station was simulated with an equivalent of 10^{11} protons, and the produced muons were then used as the initial beam in particle transport simulations of the beamlines delivering the beam to the MUH2 and MUH3 experimental areas and the beamlines' final foci.

The first HIMB *G4beamline* models were composed of *G4beamline*'s built-in particle optical elements and objects, which required lower computing resources in optimisation than using field maps. We added field maps of particle optical elements as they became available.

Target Station TgH

We performed optimisations of target TgH design and operational parameters using *G4beamline* by simulating a proton beam impinging on the target and recording the muon counts at the upstream and downstream ends of the capture solenoid in the MUH2 or MUH3 beamline, and in some cases, further downstream.

In one of the optimisations, we studied the muon flux as a function of the angles between each of the muon beamlines and the proton beamline in the horizontal plane. We also considered the counter-clockwise target rotation angles of 0, 5, and 10 degrees relative to the proton beamline. Without rotation, the target's surface would be perpendicular to the proton beam, because it is a surface muon production target. Our optimisation study confirmed the previous results that a slanted target provides a 30−60% [7] and, in one case, a ∼100% higher surface muon flux than a non-slanted target. Beamline orientations at other than 90 degrees relative to the proton beamline did not show significantly higher muon fluxes. The selected configuration uses muon beamlines placed perpendicularly to the proton beam, a 10 degree target rotation relative to the proton beamline, a 3.47 mm target thickness (providing a 20 mm proton beam path through the target), and a 100 mm target length.

We also performed optimisation studies for the aperture of a conical shield between TgH and the capture solenoid; for the use of co-directional versus contra-directional currents in the MUH2 and MUH3 capture solenoids, which are on the opposite sides of TgH; and for a non-zero incoming vertical angle of the proton beam to compensate for the magnetic field of the solenoids at the target.

We performed a particle production study for π^+ and μ^+ at TgH using *G4beamline* and *MARS*, and we recorded the particle counts at virtual detectors placed at distances 150 mm (see Fig. 2) and 250 mm from the target.

Transport Beamlines MUH2 and MUH3

The layouts of the MUH2 and MUH3 beamlines are based on maximising the muon transmission to the experiments while having at least two dipole magnets in each beamline for radiation shielding purposes. Considering the somewhat flexible constraints of the floor plans of the experimental halls, we optimised the layout of the MUH2 and MUH3 beamlines using the asynchronous Bayesian optimiser of the tool DeepHyper [11] with computing resources provided by Argonne Leadership Computing Facility, with some additional optimisation studies using grid searches. A transmission of 1.34×10^{10} muons/s in the MUH2 beamline into the experimental area was achieved. In the process of optimisations, we noticed that, as expected, the transmission tended to increase as the bending angles of the dipoles decreased.
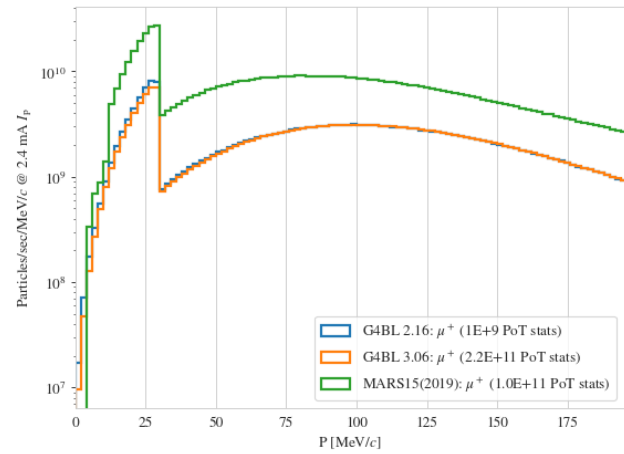

Figure 2: Muon production by target TgH, recorded 150 mm downstream from the target by a virtual detector of radius 250 mm. A comparison between *G4beamline* 3.06, *G4beamline* 2.16 (both with measured π^+ production cross-sections but with *Geant4*'s built-in π^+ decay cross-sections), and *MARS* [8, 9] is made. For a comparison of *Geant4*'s and *MARS*'s double-differential $\pi^{\pm}$ production cross-sections with experimental data, where built-in cross-sections were used for *both* codes, see Ref. [10] from the HARP collaboration.

We performed numerous optimisations of design parameters (e.g., particle optical element sequences, drift lengths, offsets, and rotations) and operational parameters (e.g., currents or fields), and studies for the design of the MUH2 and MUH3 beamlines. Optimised transmissions for MUH2 and MUH3 beamline models are shown in Figs. 3 and 4, respectively. Two examples of design studies are given in the remainder of this subsection.

We studied the possibility of using a thin aluminium or titanium degrader foil in conjunction with a downstream dipole to suppress the positron contamination, placed at an intermediate focus to reduce multiple scattering. However, our *G4beamline* simulations have shown that when these inserts are thick enough to reduce the positron contamination substantially, the muon flux is also substantially impacted. Thus, it was decided to keep the separator in the design of the MUH2 beamline for positron removal.

We studied the option of an additional branch of the MUH3 beamline for the parasitic μ^- beam, starting with a bidirectional bend at the first dipole "ASH31" of the MUH3 beamline, in the opposite directions for the μ^- and μ^+ beams. This beamline would extend for two straight sections after the dipole ASH31, use only quadrupole focusing, and provide up to $\sim 10^7$ muons/s at a proton current of 2.4 mA.

MUH2 and MUH3 Final Foci

For final focus optimisation, we calculate the transfer map of the final focus using the transfer map based code *COSY INFINITY* [12], with the quadrupole strengths and other parameters as differential-algebraic system knobs. Then
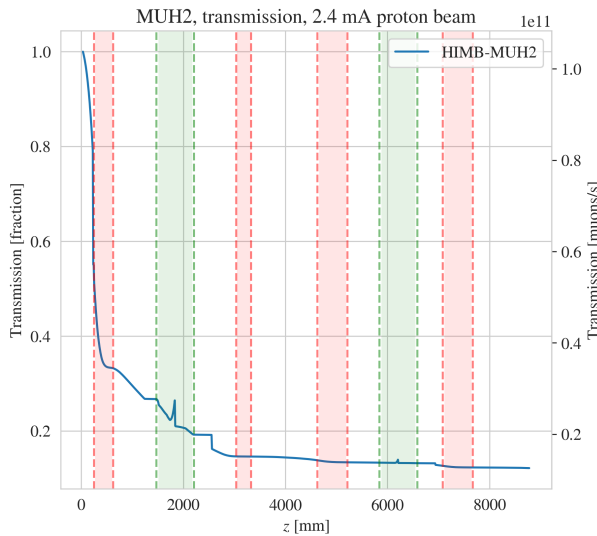
Figure 3: Muon transmission in the MUH2 beamline (preliminary model), plotted versus the longitudinal position. Dipoles and solenoids are denoted by green and red vertical columns, respectively. The optimisation of the currents was only for transmission in this case. The vertical spikes at the dipole centers are a *G4beamline* artifact due to a change in the centerline direction.
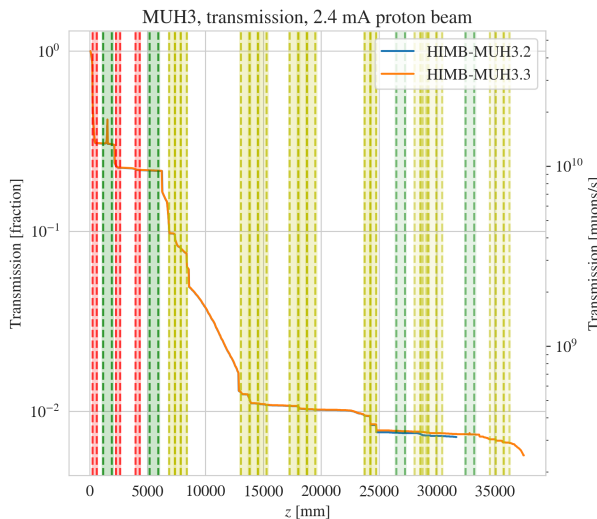

Figure 4: Muon transmission *within the momentum bite* of 25.38 to 29.79 MeV/c to the ends of the MUH3.2 (blue) and MUH3.3 branches (orange) of the MUH3 beamline (preliminary model), plotted versus the longitudinal position. Dipoles, solenoids, and quadrupoles are denoted by green, red, and yellow vertical columns, respectively. The optimisation of the currents was only for transmission in this case.

focusing is achieved by minimising the respective transfer map elements, which can be done analytically for low-order expansions in terms of the system knobs. We use *COSY INFINITY*'s built-in Levenberg–Marquardt "LMDIF" and simulated annealing optimisers.

Because the beamlines are mainly modelled using *G4beamline*, we developed a matching *COSY INFINITY* model of the *G4beamline* model of the MUH3.2 branch's final focus. The agreement between the *G4beamline* and *COSY INFINITY* models was with a difference of $\sigma(\Delta x) = 1.7$ mm and $\sigma(\Delta y) = 3.4$ mm (the latter being larger because of quite long distribution tails) for a beam passing through the MUH3.2 final focus, including a quadrupole doublet, a dipole magnet "ASS31", and a quadrupole triplet, without collimation at the entrance of the dipole. To put the differences seen between *COSY INFINITY* and *G4beamline* into context, the goal for the beam spot at the final focus is $\sigma_{x,y} \lesssim 20$ mm. The differences of 1.7 and 3.4 mm stated above are thus acceptable.

A new iteration of final focus optimisation studies is ongoing, with a field map of the dipole calculated using *Radia*.

FIELD COMPUTATIONS

The MUH3 beamline will use a horizontal steering magnet SSL32 and a septum magnet ASS31 to switch the beam delivery between the MUH3.2 and the MUH3.3 branches, with a "shared" mode where the delivery is to both. Using the boundary integral method code *Radia* [13], we computed the field maps of SSL32 and ASS31. We computed the electric field of the spin rotator SpinRot1, which is in the third straight section of the MUH3 beamline, using the boundary element method (BEM) in *COMSOL* [14]. The BEM method tends to be more accurate than the finite element method, which is also available in *COMSOL*, for such calculations.

CONCLUSION

We performed particle transport and beam optics optimisations and studies for the design of the novel HIMB beamlines at PSI, which will deliver 10^{10} muons/s to next-generation intensity frontier experiments. For that, we developed *G4beamline* models of the MUH2 and MUH3 beamlines, as well as *COSY INFINITY* and *TRANSPORT* models of parts of the MUH3 beamline[1]. We calculated the magnetic field of the dipoles SSL32 and ASS31 using the boundary integral method code *Radia* and the electric field of the spin rotator SpinRot1 using the BEM solver in *COMSOL*.

ACKNOWLEDGEMENTS

---

[1] The code *TURTLE* is also used in the HIMB project.

REFERENCES

[1] K. Arndt *et al.*, "Technical design of the phase I Mu3e experiment," *Nucl. Instrum. Methods A*, vol. 1014, p. 165 679, 2021. `doi:10.1016/j.nima.2021.165679`

[2] A. de Gouvêa and P. Vogel, "Lepton flavor and number conservation, and physics beyond the standard model," *Prog. Part. Nucl. Phys.*, vol. 71, pp. 75–92, 2013. `doi:10.1016/j.ppnp.2013.03.006`

[3] M. Aiba *et al.*, "Science Case for the new High-Intensity Muon Beams HIMB at PSI," 2021, arXiv:2111.05788 [hep-ex]. `doi:10.48550/ARXIV.2111.05788`

[4] R. Eichler *et al.*, "IMPACT conceptual design report," Paul Scherrer Institut, Report No. 22-01, 2022, `https://www.dora.lib4ri.ch/psi/islandora/object/psi:41209`

[5] Muons, Inc., *G4beamline*, version 3.06, 2019, `http://www.muonsinternal.com/muons3/G4beamline`

[6] S. Agostinelli *et al.*, "Geant4—a simulation toolkit," *Nucl. Instrum. Methods A*, vol. 506, no. 3, pp. 250–303, 2003. `doi:10.1016/S0168-9002(03)01368-8`

[7] F. Berg *et al.*, "Target studies for surface muon production," *Phys. Rev. Accel. Beams*, vol. 19, no. 2, p. 024 701, 2016. `doi:10.1103/PhysRevAccelBeams.19.024701`

[8] N. Mokhov *et al.*, "MARS15 Code Developments Driven by the Intensity Frontier Needs," *Prog. Nucl. Sci. Tech.*, vol. 4, pp. 496–501, 2014. `doi:10.15669/pnst.4.496`

[9] N. V. Mokhov and C. C. James, "The MARS code system user's guide version 15(2016)," Fermi National Accelerator Laboratory, Technical Report FERMILAB-FN-1058-APC, 2017. `doi:10.2172/1462233`

[10] M. Apollonio *et al.*, "Forward production of charged pions with incident protons on nuclear targets at the CERN Proton Synchrotron," *Phys. Rev. C*, vol. 80, p. 035 208, 3 2009. `doi:10.1103/PhysRevC.80.035208`

[11] P. Balaprakash, M. Salim, T. D. Uram, V. Vishwanath, and S. M. Wild, "DeepHyper: Asynchronous hyperparameter search for deep neural networks," in *2018 IEEE 25th International Conference on High Performance Computing (HiPC)*, 2018, pp. 42–51. `doi:10.1109/HiPC.2018.00014`

[12] K. Makino and M. Berz, "COSY INFINITY Version 9," *Nucl. Instrum. Methods A*, vol. 558, no. 1, pp. 346–350, 2006. `doi:10.1016/j.nima.2005.11.109`

[13] ESRF, *Radia*, version 4.31, 2016, `https://www.esrf.fr/Accelerators/Groups/InsertionDevices/Software/Radia`

[14] COMSOL AB, *COMSOL*, version 6.0, 2021, `https://www.comsol.com`

This is a preprint — the final version is published with IOP